Materials Research. 2022; 25:e20210083
DOI: https://doi.org/10.1590/1980-5373-MR-2021-0083

Obtaining Porous Zinc Oxide Ceramics Using Replica Technique: Application in Photocatalysis

Felipe P. Faria[a]*****, ***Thamara M. O. Ruellas***[a], ***Carolina Del Roveri***[a],
João Otávio Donizette Malafatti[b], ***Elaine Cristina Paris***[b], ***Tânia R. Giraldi***[a], ***Sylma C. Maestrelli***[a]

[a]*Universidade Federal de Alfenas, Instituto de Ciência e Tecnologia, Poços de Caldas, MG, Brasil.*
[b]*Empresa Brasileira de Pesquisa Agropecuária, Laboratório Nacional de Nanotecnologia para Agricultura (LNNA), São Carlos, SP, Brasil.*

Received: February 8, 2021; Revised: September 23, 2021; Accepted: September 26, 2021

This research investigated the production of porous zinc oxide (ZnO) ceramics obtained by the replica method for water depollution by photocatalytic processes. Five photo-decolorization cycles were performed to analyze the reuse potential of the ceramics. Statistical analyses using R programming were conducted to investigate possible significant differences between them. The ceramics porosities were between 46.74 and 62.50% (depending on the composition). The most successful results were achieved in prepared ceramics from slurries containing 65% ZnO and 1% carboxymethylcellulose, in which the dye decolorization results reached 90.5% after 5 cycles, indicating a high reuse potential of these ceramics. Multivariate analysis proved the negative effect of increasing the heat treatment temperature on the evaluated properties. The best processing conditions to obtain porous ZnO ceramics by the replica technique were established through statistical tools, with very satisfactory results in the photo-decolorization potential of the investigated dye.

Keywords: *Ceramic processing, Porosity, Rhodamine B, Advanced Oxidation Processes.*

1. Introduction

The presence of dyes in water sources and their threat to biota can be easily proven through ecotoxicological tests. Even in small concentrations, dyes can highly compromise the quality of water (about 100 μg L^{-1}). This amount is significant enough to cause the death of organisms such as water fleas and inhibit the growth of freshwater algae. These organisms are responsible for oxygen release, thus playing an important role in the maintenance of the system where they are inserted[1,2].

Industrial segments such as food production and cosmetics use dyes. However, the textile industry is the main responsible for the generation of effluents. The single-handedly textile industry releases into the environment approximately 20% of all dyes used in the dyeing of fibers and fabrics[2]. Unlike developed countries that buy their fabrics pre-dyed, emerging countries such as China, India, and Brazil dye their fabrics locally, thus generating high levels of water dye contamination[1]. The problem of dyes is aggravated by the fact that such compounds are not eliminated by conventional waste treatments[3,4]. Therefore, alternative techniques such as advanced oxidation processes (AOPs) are required. These are based on the generation of highly oxidizing species henceforth establishing favorable conditions for the degradation of such polluting substances[5-7].

Among the most commonly used materials in AOPs, ZnO stands out as an n-type semiconductor that exhibits good results in the degradation of organic compounds, such as Rhodamine B[5-9]. ZnO is a photoluminescent material in the UV range, with a density of 5.6 $g.cm^{-3}$ and a band gap of 3.37 eV at 300 K[9-15].

Through energy absorption, semiconductors enable the electronic transition between valence and conduction bands. The transition occurs when the semiconductors receive energy greater than or equal to their band gap. Therefore, successive reactions can occur on the surface of this material (referred to as photocatalyst), which constitute heterogeneous photocatalysis. In these cases, oxidizing sites are generated promoting the release of free radicals. These are responsible for the mineralization of the organic components[6-8.]

Semiconductors are generally studied in the form of ultrafine powders due to their larger surface area. This characteristic enables greater exposure to oxidizing sites and favors photocatalysis[3,8,16-18]. Nevertheless, for daily use in dye photocatalysis, it is necessary to use porous solid ceramics, which have larger surface areas than dense solids, since the material in particulate form (powders) is difficult to be recovered, compromising its regular use[18].

Porous ceramic pieces are produced through different processing routes[19-28]. Factors such as cost, ease of execution, and low waste generation can be the starting point for selecting the most appropriate processing method[22,23].

The replica method is a simple, low-cost, and widely used processing in the manufacture of porous ceramics[20,24,25]. This method consists in impregnating and drying a slurry

---

*e-mail: flipfaria@gmail.com

in a polymeric matrix (sponge) and eliminating the sponge through heat treatment. As a result, a material with porosity and structure similar to the polymeric matrix is produced[20,24,25].

The novelty of this work is based on obtaining solid porous ZnO ceramics using the replica technique for application in photocatalysis as an alternative effluent decontamination method.

2. Materials and Methods

Figure 1 illustrates the processing steps adopted to obtain porous ZnO ceramic pieces and the characterizations performed in this research.

To obtain ceramic pieces by the replica technique, an initial investigation was conducted. This was undertaken to establish the most suitable compositions that would produce stable and homogeneous ceramic suspensions (slurries) to be impregnated into the pore-forming material. Twenty different slurries were prepared with solids content between 20 and 80% w/w (ZnO powder, 99% purity, Synth®), supplemented with pure water. The organic binder Carboxymethylcellulose - CMC powder (molar mass of 240.208 g mol^{-1} and degree of substitution lower than 1, Graintec Ltda®) was also varied in contents from 1 to 5% w/w, previously diluted in warm water. The percentages were calculated in relation to a fixed final volume of 25 mL. The deflocculant content of ammonium polyacrylate (Disperlan LA, Lambra S/A®) was fixed at a weight percentile of 1% ZnO for all suspensions. After homogenization, the pH of the slips was 9. Only 12 of the initially investigated compositions produced slurries with suitable viscosities and adequate rheological properties for foam impregnation.

Table 1 shows the composition of each slurry investigated in the research after prior selection of viable compositions for foam impregnation.

Homogenization of each 25 mL slurry was performed using a Teflon flask and alumina beads in a vibrating mill (Mixer/Mill Spex Sample Prep), for 20 min, with a ball: material ratio of 5:1[18].

Thermogravimetric Analysis (TG) and Differential Scanning Calorimetry (DSC) analyses of the polyurethane foam (commercial foam, 20 pores per inch, wall thickness of 0.1 mm, and pore size ranging from 2 to 4 mm, Santa Maria Ltda®), used in this research as a pore-forming material, were performed in a Netzsch Jupiter STA 449F3 equipment with 10 mg of the material in platinum-rhodium alloy crucibles, under nitrogen atmosphere, with a heating rate of 10 K min^{-1} (-263,15 °C min^{-1}) and a temperature range of 25 to 800 °C.

The ZnO crystal structure (hexagonal wurtzite structure), along with its purity, had already been determined in a previous study[27,29]. The powders used in this previous study presented an average particle size of 0.78 µm[29]. The different slurries (12 compositions in total) were then poured onto polyurethane foams previously cut into cylindrical shapes (approximately 20 mm diameter and 5 mm thick). The foams were manually compressed to eliminate air and then immersed in the prepared suspension. This process was repeated twice for each foam to ensure good slip impregnation.

Table 1. Slurries compositions after a prior selection of viable compositions for foam impregnation.

Composition	ZnO content (% of the slurry volume)	CMC content (% of the slurry volume)
25/5	25	5
30/5	30	5
40/5	40	5
60/1	60	1
60/3	60	3
60/5	60	5
65/1	65	1
65/3	65	3
65/5	65	5
70/1	70	1
70/3	70	3
70/5	70	5

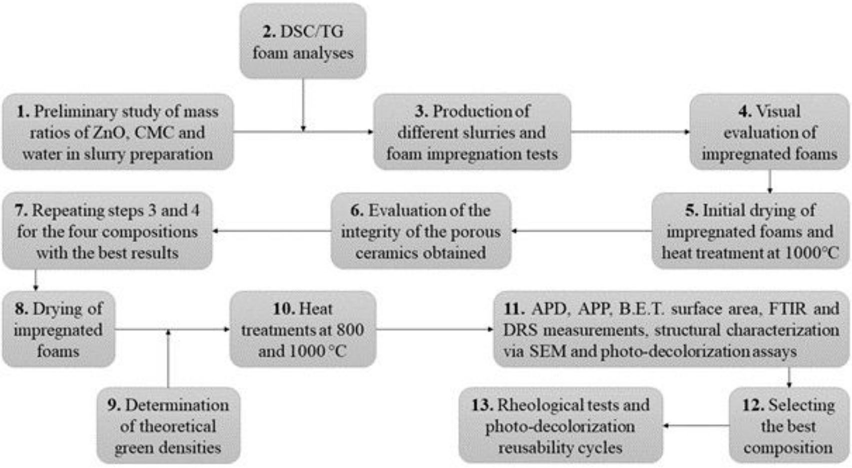

Figure 1. The processing steps performed in the research, in which CMC refers to carboxymethylcellulose, APD is the apparent density, APP is the apparent porosity, SEM is the scanning electron microscopy and DSC/TG are the exploratory differential calorimetry/ thermogravimetry analyses.

After removing the excess with a spatula, the impregnated polyurethane ceramics were dried at room temperature for 24 h. After drying, 4 compositions (60/5, 65/5, 70/3, and 70/5) presented cracks or low adhesion to the foam, which were then discarded. Thus, only the 8 slips that showed good foam impregnation continued to the subsequent heat treatment step.

The ceramics produced from these 8 different slips were heat-treated at a temperature of 1000 °C for 2 h in a muffle furnace (EDG 3000), with a heating rate of 1 °C min^{-1}. Cooling occurred at a rate of 1 °C min^{-1} until the ceramics reached room temperature. Three ceramics were prepared for each composition investigated.

The integrity of the ceramics obtained after heat treatment can be seen in Figure 2.

The slurries with up to 40% ZnO and 5% CMC generated ceramics with empty regions and voids, due to their low adhesion to the polyurethane (PU) foam, in addition to high fragility (noticeable during handling). Although CMC increases the viscosity of the slurry, the low ZnO content made it difficult to fill and bond the slurry to the PU foam, leading to high slurry loss, generating fragile ceramics that were discarded before the next steps.

Slurries containing ZnO contents above 60% were more suitable for foam impregnation due to their higher adhesion. However, compositions containing 70% ZnO and CMC above 3% did not produce a slurry, but a heterogeneous mass without fluidity, which was also discarded before the subsequent step (step 7, shown in Figure 1). The same behavior was observed for compositions with more than 60% ZnO and 5% CMC (w/w).

Slurries without any CMC content were also produced, varying only the ZnO content. None of the ceramics produced by these slurries showed physical integrity after foam impregnation followed by heat treatment at 1000 °C for 2 h. The presence of CMC was critical during the heat treatment of the ceramics. This ensured the integrity of the ceramics and cohesion among their particles during foam elimination. The preliminary study indicated that there is a strong correlation between ZnO content and CMC on the rheological properties of the slurry. For ZnO contents of approximately 70%, which contribute to the increase in viscosity, the CMC content should be approximately 1%. This is because, in addition to acting as a binder, CMC also acts as a thickener, which further increases viscosity. On the other hand, compositions with lower ZnO contents have lower viscosity and can be produced with approximately 3% CMC. In the latter case, there is no exceptionally large increase in the final viscosity, which ensures good adhesion of the slurry to the PU foam.

Thus, considering the best impregnations of the PU foam and the physical integrity of the ceramics after the sintering step, four compositions (60/3, 65/3, 65/1, and 70/1) were selected for the subsequent steps (steps 7 to 11, described in Figure 1).

New slurries obtained from the four selected compositions were prepared and impregnated with PU as described above. The green density (GD) of the ceramics was calculated according to the mixing rule, as indicated in Equation (1):

$$GD\left(g\,cm^{-3}\right)=\frac{1}{\left(\frac{x_a}{\rho_a}+\frac{x_b}{\rho_b}\right)} \tag{1}$$

where x_a and x_b correspond to the mass fractions of the foam and the slurry; ρ_a and ρ_b are their theoretical densities.

The ceramics were then heat-treated at 800 and 1000 °C for 2 h in a muffle furnace (EDG 3000), with a heating rate of 1 °C min^{-1}. Apparent porosity (APP) and apparent specific mass (APD) measurements were obtained, respectively, by Equations (2) and (3), in accordance with ABNT NBR 9778[30]:

$$APP(\%)=\left(\frac{P_{sat}-P_d}{P_{sat}-P_i}\right)*100 \tag{2}$$

$$APD\left(g\,cm^{-3}\right)=\left(\frac{P_{sat}}{P_{sat}-P_i}\right)*\rho_{H_2O} \tag{3}$$

where P_d is the dry mass of the heat-treated ceramic before being placed in water; P_i is the immersed mass; P_{sat} is the wet mass, and ρ_{H_2O} is the density of water.

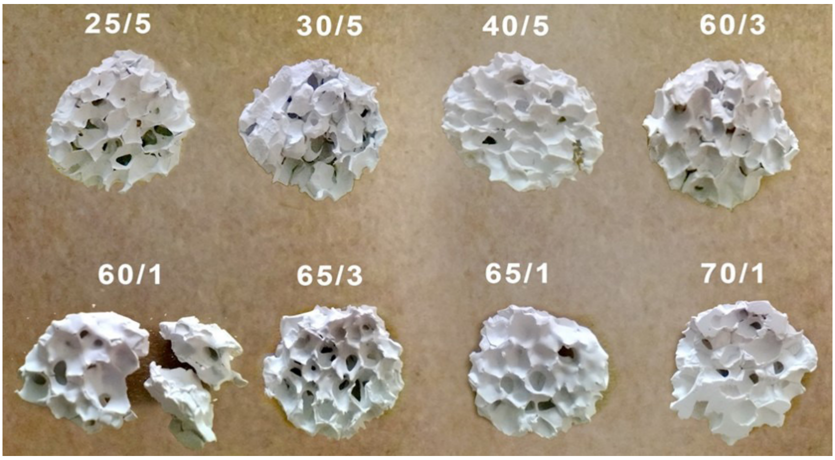

Figure 2. The integrity of heat-treated ZnO ceramics at 1000 ºC/2 h.

Microstructural characterizations of the different heat-treated compositions at 800 and 1000 °C for 2 h were performed by Scanning Electron Microscopy (SEM) using a JEOL® JSM-6010LA Compact Scanning Electron Microscope. Specific surface area analyses of the ceramics were determined by the B.E.T. method on a Micromeritics ASAP 2020 device, under N_2 flow at a temperature of 77 K.

Fourier transform infrared spectroscopy (FTIR) in reflectance mode was performed on heat-treated ceramics at 800 and 1000 °C to confirm the absence of impurities on the ZnO surface. Spectra were recorded from 400 to 4000 cm^{-1} in a Bruker® Vertex equipment with a resolution of 4 cm^{-1}. Diffuse Reflectance Spectroscopy (DRS) was conducted in a Shimadzu® RUV-2600 equipment in the 190 to 800 nm range to determine the ZnO band gap of the ceramics.

Photocatalytic decolorization was investigated through absorbance variation in a Rhodamine B (RhB, Synth®) solution. The measurements were performed in a photochemical reactor under UV-C irradiation, with four mercury vapor lamps (Philips® Ultraviolet G15T8 15 W), a cooling system with circulating water in a copper coil, through a thermostatic bath (Solab® SL152/18) at a temperature of 20.0 ± 0.1 °C. All photocatalytic experiments were performed without stirring. A schematic diagram of the photochemical reactor used in the experiments can be seen in a previously published paper by the group[28].

Before photo-decolorization, each semiconductor was immersed for 1 h in a 15 mL solution of RhB at a concentration of 5 mg L^{-1}. The calculated RhB weight percent was 0.03. The solution was also analyzed without the presence of ceramics (photolysis). All experiments were performed in triplicate, in which each system was exposed to UV-C irradiation in the reactor for 2 h, with regular interruptions every 15 min for absorbance measurement. At each analysis point, the incident UV-C irradiation inside the photochemical reactor was deactivated and an aliquot of the RhB solution was collected. The emission spectrum of the UV-C irradiation source has 3 main peaks in the UV-A (367 nm), UV-B (314 nm), and UV-C (254 nm) regions, and the irradiance at the main wavelength (254 nm) is 9.4 W m^{-2}, according to a previous study[31]. Ultraviolet-visible spectroscopy was performed in a Cary 60 UV-Vis spectrophotometer from Agilent Technologies® to analyze the dye decolorization in a glass cuvette. The scanning was performed at wavelengths from 400 to 800 nm, checking the spectral absorbance for the wavelength with the highest absorbance (554 nm). After each analysis, the aliquots were reintroduced into their respective solutions, inside the photochemical reactor, and re-exposed to UV-C irradiation. This procedure is used for photocatalytic measurements of powders and porous solid ceramics[18,27,28,32].

Five photo-decolorization cycles were also performed for the composition that presented the best photocatalytic results to verify the feasibility of its reuse. The methodology of the reuse cycles was similar to that of the photo-decolorization experiments. At the end of each cycle, the ceramics were weighed, dried at room temperature for 24 h, and resubmitted to the photocatalysis process. Simultaneously, an evaluation of the rheological properties of the slurry was carried out, which indicated the ceramics that presented the best results. The analyses were performed on an Anton Paar® MCR 72 rheometer.

Individual analyses of variance accompanied by *post hoc* tests were performed for all data. The *post hoc* analyses consist of multiple comparisons between groups of data aiming to identify the difference indicated in the analysis of variance. Furthermore, through multivariate analysis of variance, the existence of a significant difference in the mean values of the characterizations after each heat treatment (800 and 1000 ºC) was also investigated. In the latter case, the mean porosity and apparent specific mass correlated with the photocatalytic properties. All analyses were followed by individual analyses of variance and *post hoc* tests.

Statistical evaluation of all properties was established using R language, with a significance level of 0.05[33].

3. Results and Discussion

DSC/TG analyses (Figure 3) of the PU foam indicate a large mass loss from a temperature of approximately 250 to 400 °C, in which the mass percentage no longer varies. This mass loss is related to two thermal degradation phenomena. The first (250-300 ºC) is attributed to the decomposition of rigid segments (degradation of urethane bonds) with a

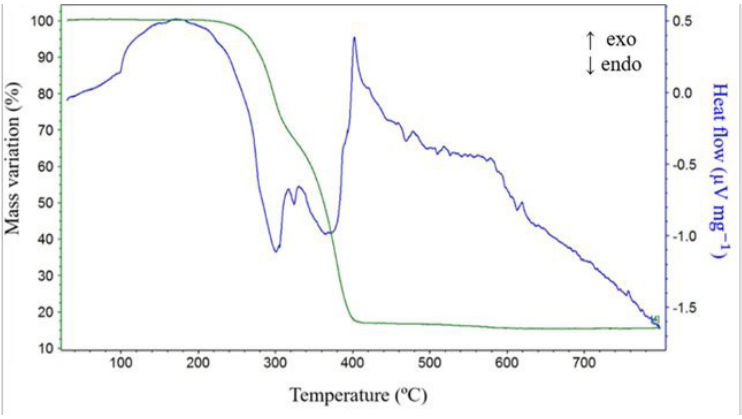

Figure 3. DSC/TG curves of the polyurethane used in the replica technique for ZnO ceramics.

mass loss of approximately 25%. The second (300-400 °C) is related to the decomposition of flexible polyurethane (polyol) segments[34-36] with a mass loss of approximately 55%. The thermal evaluation of the foam enabled an adequate configuration of the heating ramp used in the heat treatment of the different compositions, which aimed to ensure the integrity of the ZnO ceramics after foam elimination.

The preliminary analysis of the studied compositions, which considered the best foam impregnation and physical integrity of the ceramics after heat treatment, led to the selection of four compositions (60/3, 65/1, 65/3, and 70/1) for the subsequent steps (steps 7 to 11 described in Figure 1).

Table 2 shows the green density results obtained for compositions 60/3, 65/1, 65/3, and 70/1.

The green density of ceramics obtained by replica is strongly correlated with the efficiency of the slurry in filling the foam voids. Thus, homogeneous slurries with more suitable viscosity for impregnation and higher solids content better fill the voids in the foams, resulting in a higher green density.

The green density data indicate that CMC content directly influences the green density values. Additionally, lower levels of CMC added to the composition led to slightly higher green densities. CMC acts as a thickening agent (increasing the viscosity of the slurry) and helps maintain the integrity of the ceramic during heat treatment. Thus, CMC must be present in the slurry to ensure the mechanical resistance of the ceramic during heat treatment, even though it may cause a small increase in green density.

Table 2 indicates that the values for the different compositions were remarkably similar. Although the green density was increased up to 5% when increasing the solids content in the composition and/or adding lower levels of CMC.

The property under discussion was mainly affected by the CMC content. This fact is corroborated by data obtained for compositions with the same ZnO content (65/3 and 65/1) in which only the CMC content in the slurry was varied.

After heat treatment at 800 °C/2 h, the ceramics presented apparent specific mass (APD) values between 2.27 and 2.48 g cm^{-3}. For heat-treated ceramics at 1000 °C/2 h, the values ranged between 2.31 and 2.65 g cm^{-3}. This implies that ZnO heat-treated ceramics at both 800 and 1000 °C/2 h showed 41 to 46% of the ZnO theoretical density (5.61 g cm^{-3})[12], indicating that the replica technique is considerably efficient in obtaining porous ceramic pieces.

Figure 4 shows the apparent porosity values for the heat-treated ceramics at 800 and 1000 °C for 2 h.

The composition containing the highest solids content (70/1) showed the lowest apparent porosity value for both heat-treated ceramics at 800 and 1000 °C/2 h (47.3 ± 2.65 and 46.7 ± 7.52%, respectively). Such behavior was already expected since, in addition to having a higher solids content in the slurry, this composition had already shown higher green density results. Thus, the lower porosity followed the trend already presented in the green density for the composition.

Compositions with 65% ZnO obtained higher porosity indexes, which can be associated with a higher viscosity slurry, more suitable for foam filling and impregnation. After heat treatment and consequent foam removal, they presented higher and more homogeneous porosity, similar to the foam structure. The 60/3 composition also showed high apparent porosity, indicating good impregnation.

Table 2. Green density (GD) for 60/3, 65/1, 65/3, and 70/1 compositions calculated according to Equation (1).

Composition (%ZnO)/(%CMC)	**GD** (g cm^{-3})
60/3	0.95 ± 0.06
65/3	0.90 ± 0.08
65/1	1.11 ± 0.05
70/1	1.14 ± 0.05

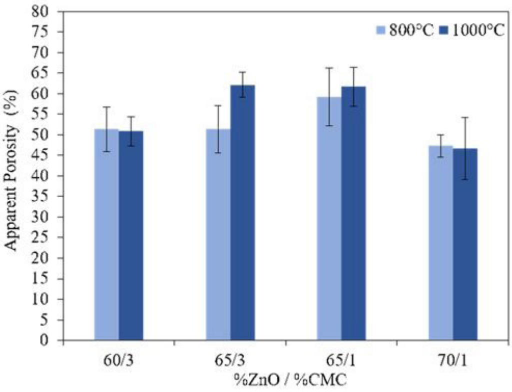

Figure 4. Apparent porosity of heat-treated ZnO ceramics at 800 ºC/2 h and 1000 ºC/2 h, in accordance with ABNT NBR 9778[29].

Figure 5 corresponds to the SEM micrographs of compositions (a) 60/3, (b) 65/3, (c) 65/1, and (d) 70/1 of heat-treated ceramics at 800 °C/2 h.

The presence of dark regions in the images obtained by SEM is related to the voids present in the microstructure (highlighted in yellow circles) indicating that the ceramics were not fully sintered. This means that the temperature used in the heat treatment did not promote the complete sintering of the pieces and the average particle size obtained in all ceramics were less than 1 µm. The 65/3 (Figure 5b) and 65/1 (Figure 5c) ceramics compositions presented higher porosity when compared to the others corroborating the results obtained for the apparent porosity.

Figure 6 corresponds to SEM micrographs of ceramics with compositions (a) 60/3, (b) 65/3, (c) 65/1, and (d) 70/1 heat-treated ceramics at 1000 °C/2 h.

Particle coalescence was observed in the heat-treated ceramics at 1000 ºC/2 h, with the appearance of necks between the particles, an intermediate step typical of the sintering process. Moreover, the average particle size was much larger than the one observed in Figure 5, greater than 2 µm, which can be explained by the increased temperature of the heat treatment.

The microstructures of heat-treated ceramics at 800 ºC/2 h (Figure 5) and 1000 ºC/2 h (Figure 6) showed that, besides the clear difference related to the average particle size, the temperature increase did not cause pore closure of compositions (a) 60/3, (b) 65/3 and (c) 65/1. They presented similar aspects, with heterogeneous particles and high porosity. For the 70/1 composition, higher levels of

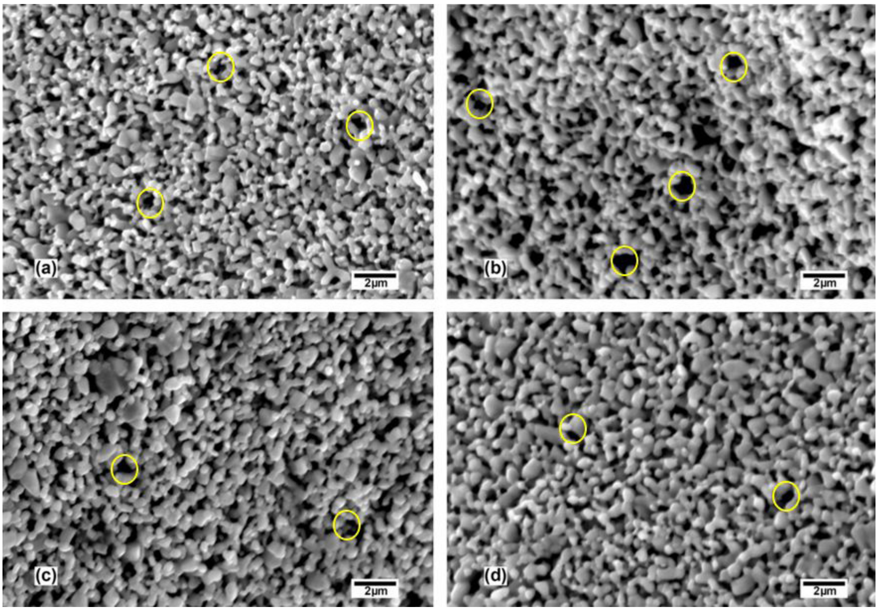

Figure 5. Micrographs of heat-treated ZnO ceramics at 800°C/2h with compositions (a) 60/3, (b) 65/3, (c) 65/1, and (d) 70/1 to evaluate the effect of temperature on porosity.

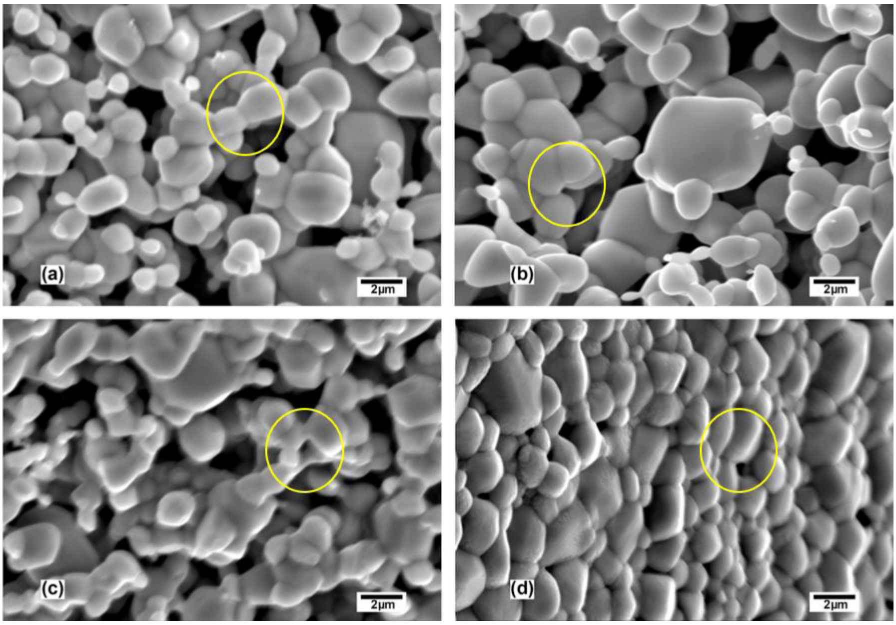

Figure 6. Micrographs of heat-treated ZnO ceramics at 1000 °C/2 h with compositions (a) 60/3, (b) 65/3, (c) 65/1, and (d) 70/1 to evaluate the effect of temperature on porosity.

densification were observed when compared to the other ceramics. The 70/1 composition was prepared with the highest content of solids (ZnO) and a higher density value was expected after heat treatment.

The micrographs obtained corroborate the apparent specific mass and apparent porosity results discussed, indicating that, except for the 70/1 composition, the ceramics showed high levels of porosity, and those heat-treated ceramics at 800 ºC/2 h presented lower average particle sizes, an important factor to be considered during photocatalysis.

Figure 7 shows the FTIR results for the heat-treated ceramics at 800 and 1000 °C for 2 h. The FTIR spectra obtained for the heat-treated ZnO ceramics were analyzed and compared with the characteristic bands of commercial ZnO and CMC.

The characteristic bands of CMC are the following: the band in the 3700–3100 cm^{-1} region is attributed to the O-H stretching, which is related to intramolecular and intermolecular hydrogen bonds. The bands at 1605 and 1437 cm^{-1} are assigned to the antisymmetric -COO stretching. The band at 1342 cm^{-1} is assigned to -CCH and -OCH coupled to the CH_2 rocking vibration, and the band at 1065 cm^{-1} is assigned to -COC vibration[37]. None of these bands were detected in the spectra of the ZnO ceramics, which proves the absence of CMC residues in them, as well as the purity of all ceramics and materials investigated. All ceramics showed a Zn-O deformation band at approximately 416 cm^{-1}, typical of the vibrational band found for the M-O bond[38,39].

Figure 8 shows the results of the DRS analysis for the heat-treated compositions at (a) 800 ºC/2 h and (b) 1000 ºC/2 h and Table 3 presents the textural analysis (B.E.T. method) and the band gap results obtained for compositions 60/3, 65/1, 65/3 and 70/1, heat-treated at 800 ºC/2 h and 1000 ºC/2 h.

The diffuse reflectance spectroscopy (DRS) results indicate that the ZnO ceramics obtained at 800 °C/2 h and 1000 °C/2 h showed band gap results between 3.2 and 3.3 eV. These results are similar to those found in the literature[28,38] for the oxide. The heat-treated ceramics at a higher temperature (1000 °C) showed lower values when compared to those heat-treated ceramics at 800 °C. The band gap energy results are significantly influenced by the treatment temperature due to variations in particle size, electron carrier concentration, and oxygen vacancies in the conduction band. In addition, higher temperatures promote an increase in crystallinity and particle size, decreasing the number of structural defects and the *band gap* results[40]. Therefore, the decrease in the band gap results of ZnO ceramics from 3.3 eV to 3.2 eV is in agreement with the variation of the heat treatment temperature from 800 to 1000 °C.

The B.E.T. results indicate that heat-treated compositions at 800 ºC/2 h have higher specific surface areas than those heat-treated ceramics at 1000 ºC/2 h. The 70/1 composition presented the lowest surface area results for ceramics treated at 800 ºC/2 h (1.857 m^2 g^{-1}) and ceramics treated at 1000 ºC/2 h

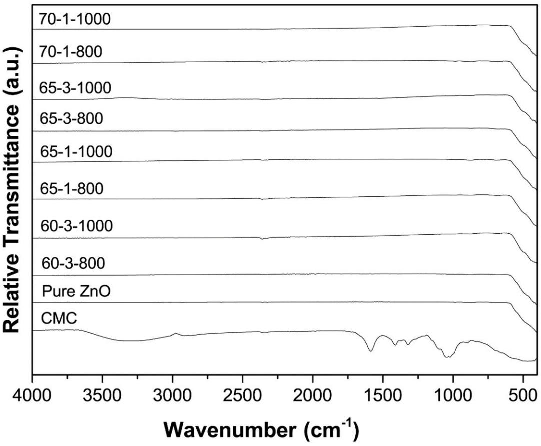

Figure 7. FTIR spectra for heat-treated ZnO ceramics at 800 °C/2 h and 1000 °C/2 h.

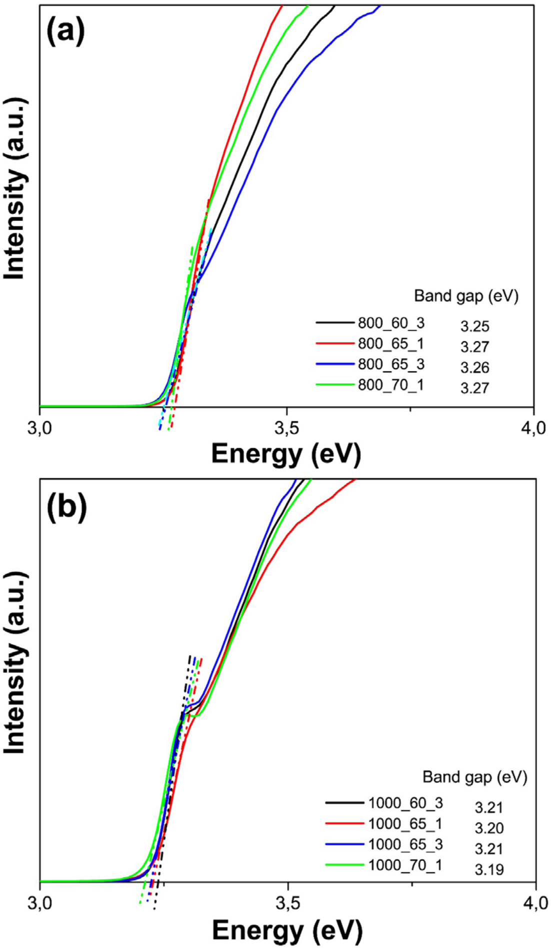

Figure 8. DRS results for heat-treated compositions at (a) 800 ºC/2 h and (b) 1000 ºC/2 h.

Table 3. Textural analysis (B.E.T. surface area) and band gap of 60/3, 65/1, 65/3, and 70/1 heat-treated ZnO compositions at 800 ºC/2 h and 1000 ºC/2 h.

Heat treatment	ZnO Composition	B.E.T. surface area (m^2 g^{-1})	Band gap (eV)
800 ºC/2 h	60/3	1.976	3.25
	65/3	1.893	3.26
	65/1	1.962	3.27
	70/1	1.857	3.27
1000 ºC/2 h	60/3	0.616	3.21
	65/3	0.594	3.21
	65/1	0.680	3.20
	70/1	0.388	3.19

(0.388 m^2 g^{-1}). The lower porosity of this composition (seen in Figure 4 and micrographs), along with the lower surface area, negatively influences the photocatalytic properties due to lower exposure to irradiation in the material. The 70/1 composition presents a surface area for heat-treated ceramics at 1000 ºC/2 h up to 4 times smaller than those for heat-treated ceramics at 800 ºC/2 h, which directly impacts its photocatalytic results.

The 65/1 composition exhibited the highest porosity when compared to the other compositions. The surface area of the heat-treated ceramics at 800 ºC/2 h (1.962 m^2 g^{-1}) was approximately 35% higher than the results obtained for the ceramics treated at 1000 ºC/2 h (0.680 m^2 g^{-1}). The high porosity achieved and the larger surface area of this composition, when compared to the others, directly influenced the photocatalytic properties.

Figure 9 shows the results obtained from the photocatalytic experiments for the heat-treated compositions at (a) 800 ºC/2 h and (b) 1000 ºC/2 h and Table 3 shows the decolorization percentage obtained for compositions 60/3, 65/1, 65/3 and 70/1, heat-treated ceramics at 800 and 1000 ºC/2 h, with their respective masses.

Heat-treated ceramics at 800 ºC/2 h showed a higher decolorization capacity than those heat-treated ceramics at 1000 ºC/2 h. All heat-treated ceramics showed high degrees of porosity. However, particle coalescence resulted from increasing the heat treatment temperature to 1000 ºC/2 h, causing the specific surface area to decrease, as observed in the B.E.T results. This led to a smaller area of exposure to UV-C irradiation for the heat-treated ceramics at 1000 ºC/2 h and therefore lower photocatalytic activity.

Porosity and specific surface area strongly influenced the photo-decolorization potential. The 65/1 composition, which had the highest porosity levels, was also the one with the best decolorization results of 64.6% and 41.4% for heat-treated ceramics at 800 and 1000 ºC, respectively, as discussed previously.

The results obtained for the 70/1 composition, in which the ceramics were heat-treated at 1000 ºC/2 h, also corroborate the influence of porosity on dye decolorization, since the microstructure obtained under these conditions was less porous and presented lower specific surface area, with the lowest decolorization percentages.

Figure 10 shows the radar chart for compositions 60/3, 65/3, 65/1, and 70/1 heat-treated ceramics at (a) 800 °C/2 h and (b) 1000 ºC/2 h concerning the evaluated properties. The radar chart aimed to quickly evaluate the quantitative variables green density, apparent porosity, and decolorization of each composition, and represent them on axes starting from

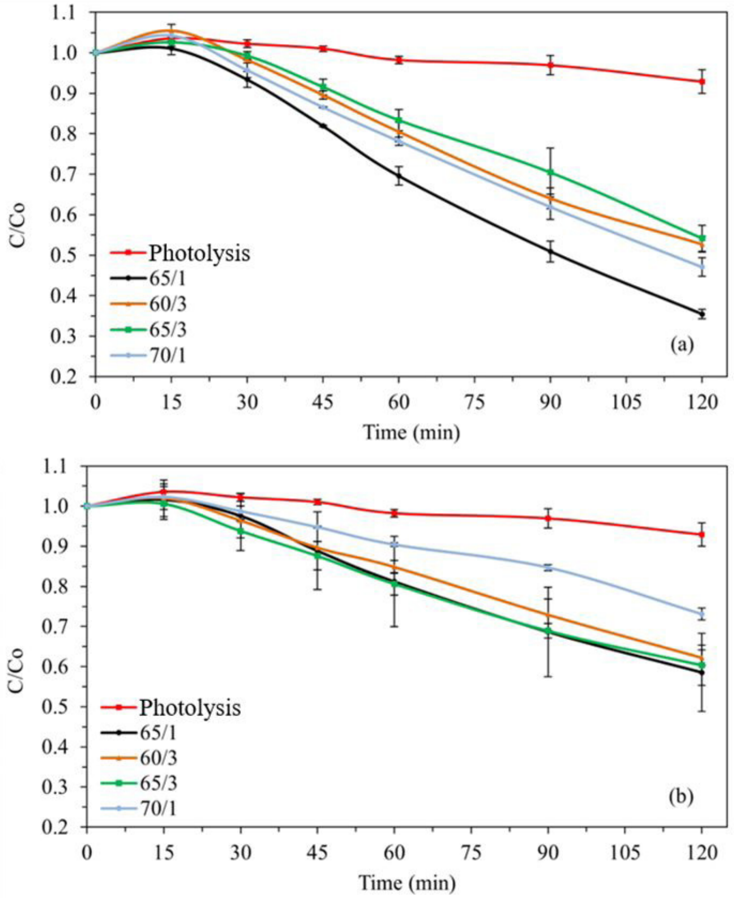

Figure 9. Rhodamine B (5 mg L^{-1}) photo-decolorization as a function of time in the presence of heat-treated ZnO ceramics at (a) 800 °C/ 2h and (b) 1000 °C/ 2h.

the same point. The optimal conditions were parameterized considering maximum decolorization (100%), minimum green density results (10%), and 90% apparent porosity (which corresponds to the highest apparent porosity value obtained, regardless of the technique and ceramic material investigated).

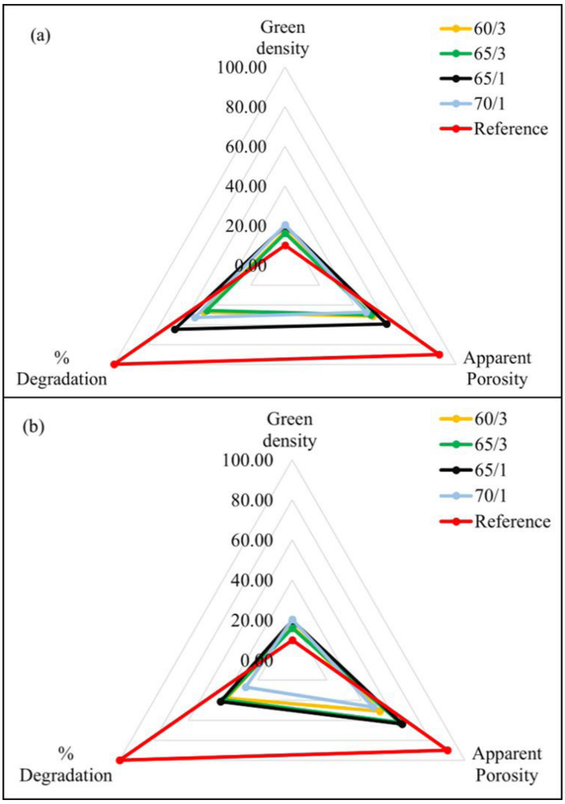

Figure 10. Radar chart for compositions 60/3, 65/3, 65/1, and 70/1 heat-treated at (a) 800 °C/2 h and (b) 1000 ºC/2 h regarding the evaluated properties.

The radar chart images establish that, for both heat treatments, the 65/1 composition was closest to the optimal results (black line). Therefore, this composition was selected for the following stages of the research, in which the results were also evaluated over 5 photo-decolorization cycles.

Table 4 and Figure 11 show the results of the photo-decolorization cycles performed on the 65/1 composition. In the last cycle, the photo-decolorization was maintained and there were no further significant mass variations.

The results indicate that the ceramics were reusable for at least 5 cycles. It is important to consider that synthesis residue adsorbed on the photocatalyst surface can compete with oxidizing sites and impair photocatalytic efficiency[27,28]. This did not seem to affect the process, as there was no considerable reduction in decolorization. In addition, an increase in the percentage of dye decolorization was observed in comparison to the first cycles. The decolorization percentages shown in Table 5 indicate an increase in photocatalytic activity until stabilization, showing that excellent levels of photo-decolorization were achieved.

Bearing in mind that the photo-decolorization improvement occurred until the third cycle, the mass loss of one of these pieces was measured after the first three reuse cycles. There was a loss of approximately 50 mg of ZnO. Some of this loss may have originated from the handling of the ceramic. However, considering that a small amount of ZnO is indeed present in the suspension, the increase in photo-decolorization after this mass loss is mainly associated with the presence

Table 4. Results of decolorization levels after 5 cycles of photocatalysis of 65/1 heat-treated ZnO composition at 1000 °C/2 h.

Cycle	Achieved decolorization level (%)
1	63.64 ± 2.99
2	79.66 ± 4.88
3	90.45 ± 2.07
4	82.74 ± 1.94
5	82.72 ± 2.22

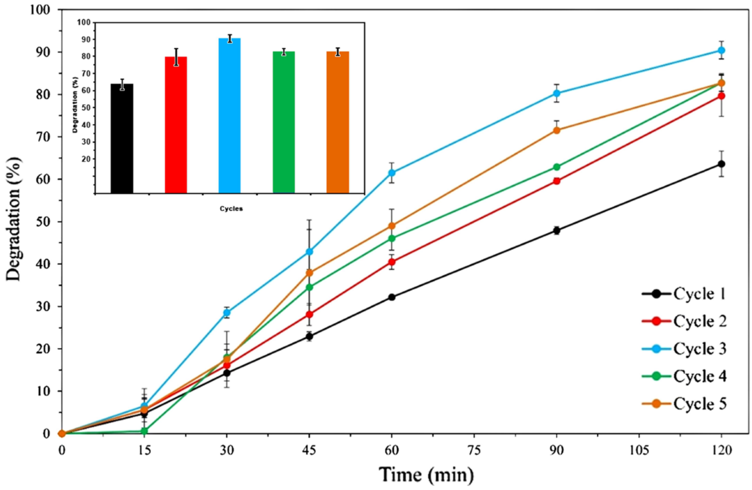

Figure 11. Photo-decolorization percentage after each photocatalytic cycle in the presence of the 65/1 heat-treated ZnO composition at 1000 °C/2 h.

Table 5. Decolorization results obtained after photocatalytic experiments of 60/3, 65/3, 65/1, and 70/1 heat-treated ZnO compositions at 800 ºC/2 h and 1000 ºC/2 h.

Composition (%ZnO)/(%CMC)	800 ºC/2 h		1000 ºC/2 h	
	Mean mass (g)	Decolorization (%)	Mean mass (g)	Decolorization (%)
60/3	2.31 ± 0.05	47.30	2.11 ± 0.03	37.80
65/3	2.37 ± 0.03	45.84	1.78 ± 0.03	39.65
65/1	2.97 ± 0.03	64.55	2.72 ± 0.04	41.45
70/1	2.95 ± 0.04	52.92	3.09 ± 0.05	26.91

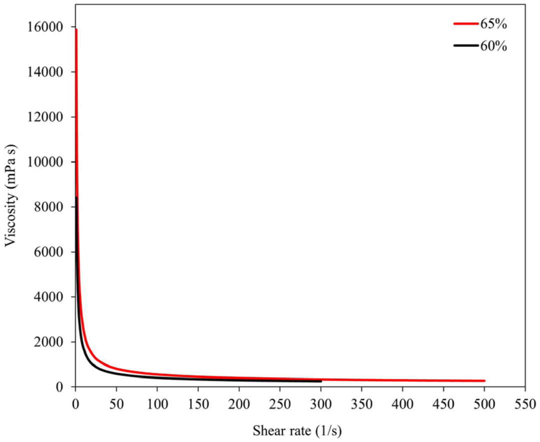

Figure 12. Viscosity curves for the 65/1 and 60/1 composition slurries obtained after homogenization in vibrating mill for 20 min.

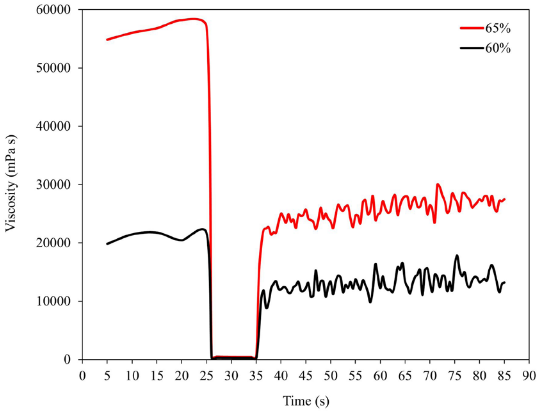

Figure 13. Time-dependent behavior for the 65/1 and 60/1 composition slurries obtained after homogenization in vibrating mill for 20 min.

of particulate ZnO in the suspension, because of its high surface area and higher mass transfer[41-44].

Ruellas et al.[28] obtained ZnO pieces by slip casting and pressing with mean porosities of 44.87 and 1.56%, respectively. Ceramics obtained by slip casting achieved photo-decolorization levels between 80 and 90%, whereas the pieces produced by pressing showed 40 to 60% photo-decolorization. Rangel et al.[44] obtained homogeneously distributed pores in nanostructured ZnO particles deposited on a glass foam synthesized hydrothermally via microwave. However, the achieved photo-decolorization levels were considerably low (below 40%).

In another study[27], the authors reached 40% porosity in pieces also obtained by slip casting with approximately 89% of photocatalysis. The porosity results of this research are higher than the results obtained in other works cited above. Nevertheless, the pieces obtained by the replica technique enabled an increase in the photo-decolorization of the dye.

Figure 12 shows the viscosity curve as a function of the applied shear rate for the 65/1 composition. For comparison purposes, the same test was performed for the 60/1 composition. The ceramics of both compositions show a limit strain on the curve from which the viscosity does not vary and are classified as Bingham plastic fluids.

Figure 13 refers to the determination of the viscosity as a function of time. From the results, both ZnO slurries are classified as rheopexy fluids, as they show an increase in viscosity over time, which favors the fixation of the suspension in the foam until the end of the drying step. Additionally, the 65/1 composition shows a much faster increase in its slurry viscosity compared to the 60/1 composition. Although a lower viscosity favors the filling of foam voids, the faster viscosity recovery makes the slurry more efficient to integrate porous mold and prevents losses, which made the 65% ZnO ceramics perform better.

The discussions presented were all corroborated by the statistical analyzes performed. For the green density averages, the analyses of variance, accompanied by *post hoc* tests, confirmed the active influence of CMC content on viscosity regulation. As observed experimentally, ceramics produced with a variation of ZnO content, for the same CMC content, were statistically similar in terms of green density.

On the other hand, for the multivariate analyses, there was a statistically significant difference in the properties considered for the two heat treatments. The calculated significance level was 0.0007 for the set of heat-treated ceramics at 800 ºC and 0.0004 for the set at 1000 ºC.

Individual analyses of variance followed by *post hoc* tests were additionally used in the evaluation of the properties that varied with the different compositions. First, concerning porosity, for both heat treatments, the ceramics that were produced with 65% ZnO had a different statistical behavior than the others. This result reinforces the microscopy images presented, along with the discussions in Figure 4. The existence of a more suitable slurry composition capable of producing ceramics with high porosity levels was verified in comparison with the other suspensions tested.

Furthermore, the heat treatment performed at 800 ºC did not produce a significant difference in the apparent specific mass of the prepared ceramics. In this case, the average values were statistically similar. However, for the temperature of 1000 ºC, the experimental suspensions made it possible to obtain ceramics with different apparent specific masses. Figures 5 and 6 corroborate this result, indicating greater structural changes for the heat treatment at 1000 °C.

Finally, when considering the photo-decolorization properties, for the two heat treatment temperatures evaluated, the slurry with 65% ZnO and 1% CMC showed a different statistical behavior among the others. The statistical treatment applied confirms all the information presented in the physical and microstructural characterizations of the ceramics obtained by the replica technique.

4. Conclusions

The replica technique investigated in this work enabled the production of ZnO ceramics with high porosity. In general, the heat-treated ceramics at 800 and 1000 ºC presented high levels of porosity (above 45% for all compositions). The highest surface areas were those of the heat-treated ceramics at 800 ºC, which resulted in the best photocatalysis results.

The individual and multivariate analyses of variance proved the influence of the heat treatment temperature on the physical properties and microstructure of the produced ceramics. Furthermore, they corroborated the superior behavior of the 65/1 composition ceramics for all investigated properties.

Slurries with 65% ZnO and 1% CMC originated ceramics with the highest porosity that reached remarkably high levels of Rhodamine B decolorization (90.5%) after 5 cycles which implies a high reusability potential of these ceramics. Thus, the ceramics produced by the replica technique in this research proved to be reusable.

5. Acknowledgements

The authors gratefully acknowledge Conselho Nacional de Desenvolvimento Científico e Tecnológico (CNPq), Empresa Brasileira de Pesquisa Agropecuária (EMBRAPA), Fundação de Amparo à Pesquisa do Estado de Minas Gerais (FAPEMIG), Universidade Estadual Paulista (UNESP *campus* Rio Claro) and Universidade Federal de Alfenas (UNIFAL-MG), for the technical and financial support.

6. References

1. Carneiro PA, Umbuzeiro GA, Oliveira DP, Zanoni MVB. Assessment of water contamination caused by a mutagenic textile effluent/dyehouse effluent bearing disperse dyes. J Hazard Mater. 2010;174:694-9. http://dx.doi.org/10.1016/j.jhazmat.2009.09.106.
2. Brites FF, Machado NRC, Santana VS. Effect of support on the photocatalytic degradation of textile effluents using Nb_2O_5 and ZnO: photocatalytic degradation of textile dye. Top Catal. 2011;54:264-9. http://dx.doi.org/10.1007/s11244-011-9657-2.
3. González-Rodríguez J, Fernández L, Bava YB, Buceta D, Vázquez-Vázquez C, López-Quintela MA, et al. Enhanced photocatalytic activity of semiconductor nanocomposites doped with Ag nanoclusters under UV and visible light. Catalysts. 2020;10:31. http://dx.doi.org/10.3390/catal10010031.
4. Lops C, Ancona A, Cesare K, Dumontel B, Garino N, Canavese G, et al. Sonophotocatalytic degradation mechanisms of Rhodamine B dye via radicals generation by micro- and nano-particles of ZnO. Appl Catal B. 2019;243:629-40. http://dx.doi.org/10.1016/j.apcatb.2018.10.078.
5. Pivert ML, Poupart R, Capochichi-Gnambodoe M, Martin N, Leprince-Wang Y. Direct growth of ZnO nanowires on civil Engineering materials: smart materials for supported Photodegradation. Microsyst Nanoeng. 2019;5:57. http://dx.doi.org/10.1038/s41378-019-0102-1.
6. Melinte V, Stroea L, Chibac-Scutaru AL. Polymer nanocomposites for photocatalytic applications. Catalysts. 2019;9(12):986. http://dx.doi.org/10.3390/catal9120986.
7. Zhu YF, Zhou L, Jiang QS. One-dimensional ZnO nanowires grown on three-dimensional scaffolds for improved photocatalytic activity. Ceram Int. 2020;46:1158-63. http://dx.doi.org/10.1016/j.ceramint.2019.09.084.
8. Thirukumaran P, Atchudan R, Parveen AS, Kalaiarasan K, Lee YR, Kim SC. Fabrication of ZnO Nanoparticles adorned nitrogen-doped carbon balls and their application in Photodegradation of organic dyes. Sci Rep. 2019;9:19509.
9. Luna-Flores A, Morales MA, Agustín-Serrano R, Portillo R, Luna-López JA, Pérez-Sánchez GF, et al. Improvement of the photocatalytic activity of ZnO/Burkeite heterostructure prepared by combustion method. Catalysts. 2019;9:817. http://dx.doi.org/10.3390/catal9100817.
10. Wang LZ. Zinc oxide nanostructures: growth, properties and applications. J Phys Condens Matter. 2004;16:829-58. http://dx.doi.org/10.1088/0953-8984/16/25/R01.
11. Mayrinck C, Ferrari JL, Raphael E, Schiavon MA. Synthesis, properties and applications of nanostructured zinc oxide. Virtual Química. 2014;6:1185-204. http://dx.doi.org/10.5935/1984-6835.20140078.
12. Özgür Ü, Liu C, Alivov Y, Teke A. A comprehensive review of ZnO materials and devices. J App Phys. 2005;98(4):041301. https://doi.org/10.1063/1.1992666.
13. Bolzon LP, Costa L, Moura A, Pedroso C, Prado AGS. Nb_2O_5 as efficient and recyclable photocatalyst for indigo carmine degradation. Environ. 2008;82:219-24. http://dx.doi.org/10.1016/j.apcatb.2008.01.024.
14. Ribeiro A, Pereira MFR, Nunes OC, Silva AMT. An overview on the advanced oxidation processes applied for the treatment of water pollutants defined in the recently launched Directive 2013/39/EU. Environ Int. 2015;75:33-51. http://dx.doi.org/10.1016/j.envint.2014.10.027.
15. Araujo FVDF, Yokoyama L, Teixeira LA. Color removal in reactive dye solutions by UV/H_2O_2 oxidation. Quim Nova. 2006;29:11-4. http://dx.doi.org/10.1590/S0100-40422006000100003.
16. Bezerra PCS, Cavalcante RP, Garcia A, Wender H, Martines MAU, Casagrande GA, et al. Synthesis, characterization and photocatalytic activity of pure and N-, B-, or A- doped TiO_2. J Braz Chem Soc. 2017;28:1788-802. http://dx.doi.org/10.21577/0103-5053.20170040.
17. Pipi A, Byzynski G, Ruotolo L. Photocatalytic activity and RNO dye degradation of nitrogen-doped TiO_2 prepared by ionothermal synthesis. Mater Res. 2017;20:628-38. http://dx.doi.org/10.1590/1980-5373-mr-2016-0837.
18. Gonçalves P, Bertholdo R, Dias JA, Maestrelli SC, Giraldi TR. Evaluation of the photocatalytic potential of TiO_2 and ZnO obtained by different wet chemical methods. Mater Res. 2017;20:181-9. http://dx.doi.org/10.1590/1980-5373-mr-2016-0936.
19. Matsuzawa S, Maneerat C, Hayata Y, Hirakawa T, Negishi N, Sano T. Immobilization of TiO_2 nanoparticles on polymeric substrates by using electrostatic interaction in the aqueous phase. Appl Catal B. 2008;83:39-45. http://dx.doi.org/10.1016/j.apcatb.2008.01.036.
20. Colombo P. Conventional and novel processing methods for cellular ceramics. Philosophical Transactions of the Royal Society A. 2006;364:109-24. http://dx.doi.org/10.1098/rsta.2005.1683.
21. Studart AR, Gonzenbach UT, Tervoort E, Gauckler LJ. Processing routes to macroporous ceramics: a review. J Am Ceram Soc. 2006;89:1771-89. http://dx.doi.org/10.1111/j.1551-2916.2006.01044.x.
22. Sepulveda P, Binner JGP. Processing of cellular ceramics by foaming and in situ polymerization of organic monomers. J

Eur Ceram Soc. 1999;19:2059-66. http://dx.doi.org/10.1016/S0955-2219(99)00024-2.

23. Aleni AH, Kretzschmar N, Jansson A, Ituarte IF, St-Pierre L. 3D printing of dense and porous TiO_2 structures. Ceram Int. 2020;46:16725-32. http://dx.doi.org/10.1016/j.ceramint.2020.03.248.
24. Ishii K, Shimizu M, Sameshima H, Samitsu S, Ishigaki T, Uchikoshi T. Fabrication of porous $(Ba,Sr)(Co,Fe)O_{3-\delta}$ (BSCF) ceramics using gelatinization and retrogradation phenomena of starch as pore-forming agent. Ceram Int. 2020;46:13047-53. http://dx.doi.org/10.1016/j.ceramint.2020.02.075.
25. Colombo P, Bernardo E. Macro and micro-cellular porous ceramics from preceramic polymers. Compos Sci Technol. 2003;63:2353-9. http://dx.doi.org/10.1016/S0266-3538(03)00268-9.
26. Romano RCO, Pandolfelli VC. Production and properties of porous ceramics obtained by foam addition technique. Ceramica. 2006;52:213-9. http://dx.doi.org/10.1590/S0366-69132006000200015.
27. Ruellas TMO, Peçanha LOO, Domingos GHS, Maestrelli SC, Giraldi TR. Photodegradation of Rhodamine B catalyzed by ZnO pellets. Ceramica. 2019;65:47-53. http://dx.doi.org/10.1590/0366-6913201965s12609.
28. Ruellas TMO, Peçanha LOO, Domingos GHS, Sciena CS, Malafatti JOD, Paris EC, et al. Zinc oxide pieces obtained by pressing and slip casting: physical, structural and photocatalytic properties. Environ Technol. 2019;42(12): 1861-73. http://dx.doi.org/10.1080/09593330.2019.1683078.
29. Dias JA, Ramos AS, Minucci MZ, Giraldi TR, Arantes VL, Maestrelli SC. Characterization and photocatalytic evaluation of ZnO-Co_3O_4 particles obtained by high energy milling. Part I: Processing, physicochemical and thermal characterization. Ceram Int. 2016;42:1425-31. http://dx.doi.org/10.1016/j.ceramint.2015.09.086.
30. ABNT: Associação Brasileira de Normas Técnicas. NBR 9778: Hardened cement mortar and concrete - Determination of water absorption by immersion. Rio de Janeiro: ABNT; 1995.
31. Moreira AJ, Borges AC, Sousa BB, Mendonça VR, Freschi CD, Freschi GPG. Photodegradation of fluoxetine applying different photolytic reactors: evaluation of the process efficiency and mechanism. J Braz Chem Soc. 2019;30:1010-24. http://dx.doi.org/10.21577/0103-5053.20180250.
32. Dias JA, Ramos AS, Minucci MZ, Giraldi TR, Arantes VL, Maestrelli SC. Characterization and photocatalytic evaluation of ZnO-Co_3O_4 particles obtained by high energy milling. Part II: photocatalytic properties. Ceram Int. 2016;42:3485-90. http://dx.doi.org/10.1016/j.ceramint.2015.10.151.
33. Field A, Miles J, Field Z. Discovering statistics using R. Thousand Oaks: SAGE; 2012.
34. Mothé CG, Araujo CR. Caracterização térmica e mecânica de compósitos de poliuretano com fibras de Curauá. Polímeros. 2004;14(4):274-8. http://dx.doi.org/10.1590/S0104-14282004000400014.
35. Cervantes-Uc JM, Espinosa JIM, Cauich-Rodríguez JV, Ávila-Ortega A, Vázquez-Torres H, Marcos-Fernández A, et al. TGA/FTIR studies of segmented aliphatic polyurethanes and their nanocomposites prepared with commercial montmorillonites. Polym Degrad Stabil. 2009;94(10):1666-77. http://dx.doi.org/10.1016/j.polymdegradstab.2009.06.022.
36. Herrera M, Matuschek G, Kettrup A. Thermal degradation of Thermoplastic Polyurethane Elastomers (TPU) based on MDI. Polym Degrad Stabil. 2002;78(2):323-31. http://dx.doi.org/10.1016/S0141-3910(02)00181-7.
37. Xiong J, Li Q, Shi Z, Ye J. Interactions between wheat starch and cellulose derivatives in short-term retrogradation: Rheology and FTIR study. Int Food Res J. 2017;100(P1):858-63. https://doi.org/10.1016/j.foodres.2017.07.061.
38. Domingos GHS, Ruellas TMO, Peçanha LOO, Malafatti JOD, Paris EC, Maestrelli SC, et al. ZnO semiconductors obtained by slip casting: application and reuse in photocatalysis. Int J Appl Ceram Technol. 2020;18:622-30. http://dx.doi.org/10.1111/ijac.13698.
39. Pereira FF, Paris EC, Bresolin JD, Mitsuyuki MC, Ferreira MD, Corrêa DS. The effect of ZnO nanoparticles morphology on the toxicity towards microalgae Pseudokirchneriella subcapitata. J Nanosci Nanotechnol. 2020;20(1):48-63. http://dx.doi.org/10.1166/jnn.2020.16880.
40. Omri K, Najeh I, Dhahri R, El Ghoul J, El Mir L. Effects of temperature on the optical and electrical properties f ZnO nanoparticles synthesized by sol-gel method. Microelectron Eng. 2014;128:53-8. http://dx.doi.org/10.1016/j.mee.2014.05.029.
41. Erdem E. Microwave power, temperature, atmospheric and light dependence of intrinsic defects in ZnO nanoparticles: A study of electron paramagnetic resonance (EPR) spectroscopy. J Alloys Compd. 2014;605:34-44. http://dx.doi.org/10.1016/j.jallcom.2014.03.157.
42. Kaftelen H, Ocakoglu K, Thomann R, Tu S, Weber S, Erdem E. EPR and photoluminescence spectroscopy studies on the defect structure of ZnO nanocrystals. Phys Rev B. 2012;86(1):014113. http://dx.doi.org/10.1103/PhysRevB.86.014113.
43. Baraki R, Zierep P, Erdem E, Weber S, Granzow T. Electron paramagnetic resonance study of ZnO varistor material. J Phys Condens Matter. 2014;26(11):115801. http://dx.doi.org/10.1088/0953-8984/26/11/115801.
44. Rangel EM, Melo CCN, Machado FM. Ceramic foam decorated with ZnO for photodegradation of Rhodamine B dye. Bol Soc Esp Ceram Vidr. 2019;58:134-40. http://dx.doi.org/10.1016/j.bsecv.2018.10.002.